Applied Catalysis B: Environmental 88 (2009) 368–375

Contents lists available at ScienceDirect

Applied Catalysis B: Environmental

journal homepage: www.elsevier.com/locate/apcatb

# Hollow core/mesoporous shell carbon capsule as an unique cathode catalyst support in direct methanol fuel cell

Jung Ho Kim, Baizeng Fang, Suk Bon Yoon, Jong-Sung Yu *

*Department of Advanced Materials Chemistry, BK21 Research Team, Korea University, 208 Seochang, Jochiwon, ChungNam 339-700, Republic of Korea*

ARTICLE INFO

*Article history:*
Received 25 April 2008
Received in revised form 13 October 2008
Accepted 3 November 2008
Available online 12 November 2008

*Keywords:*
Hollow core mesoporous shell carbon
Electrocatalyst
Catalyst support
Oxygen reduction reaction
Direct methanol fuel cell

ABSTRACT

Hollow core mesoporous shell (HCMS) carbon has been explored for the first time as a cathode catalyst support in direct methanol fuel cells (DMFCs). The HCMS carbon consisting of discrete spherical particles possesses unique structural characteristics including large specific surface area and mesoporous volume and well-developed interconnected void structure, which are highly desired for a cathode catalyst support in low temperature fuel cells. Significant enhancement in the electrocatalytic activity toward oxygen reduction reaction has been achieved by the HCMS carbon-supported Pt nanoparticles compared with carbon black Vulcan XC-72-supported ones in the DMFC. In addition, much higher power was delivered by the Pt/HCMS catalysts (i.e., corresponding to an enhancement of ca. 91–128% in power density compared with that of Pt/Vulcan), suggesting that HCMS carbon is a unique cathode catalyst support in direct methanol fuel cell.



## 1. Introduction

Direct methanol fuel cell (DMFC) has been considered promising power sources for portable applications because of its high energy density for fuel storage and simplicity of its subsystem requirements [1–9]. However, one of the major barriers for the commercialization of DMFC is the low catalyst activities, especially toward oxygen reduction reaction (ORR) in cathode part since the kinetics of the ORR is extremely sluggish even at Pt catalysts, resulting in a significant voltage loss at the Pt cathode. It has been reported that the specific activities of the platinum-based catalysts toward the ORR are considerably related to their supporting materials, mainly porous carbonaceous materials [10–12]. Thus, one strategy to enhance the activity of the ORR is to explore highly active catalysts with novel carbon support. It is well known that ideal supporting materials should have the following basic characteristics such as high electrical conductivity, well-developed pore structure, large surface area and pore volume. Carbon black, such as Vulcan XC-72 (VC), has been the most widely used as a catalyst support because of its relatively good compromise between electronic conductivity and surface area [13–15]. However, the VC carbon exhibits broad pore size distribution and poor pore connectivity, which may limit the performance of the supported catalysts. Recently, new nanostructured carbon materials such as carbon nanotubes (CNTs) [16–19], nitrogen containing CNT [20], nanofibers [21–23], nanohorns [24], nanoporous arrays [25–28], and carbon microbeads [29] have been studied as supporting materials mainly for the anode catalysts. Improved catalytic activities toward methanol oxidation have been reported for their supported catalysts compared with their commercial counterparts. In our previous work, hollow core mesoporous shell (HCMS) carbon has shown higher catalytic activity toward methanol oxidation and enhanced power density than the VC under the identical DMFC anode operation conditions [30]. Although that, a question still remained if this material would be suitable to support Pt as a cathode catalyst in DMFC due to its considerably different oxidative operation environment. It is very important and significant to enhance the activity of the Pt catalyst toward ORR and improve fuel cell polarization performance by catalyst support technology particularly in DMFC with air-fed cathode mode. However, little study has been done in cathode catalyst support, which plays more crucial role in the DMFC performance. In addition, core size and (or) shell thickness of the HCMS carbon may have impacts on the fuel cell performance of the supported Pt cathode catalysts. In this paper, the HCMS carbon materials with various core size and (or) shell thickness were prepared and explored as DMFC cathode supports. Much higher catalytic activity toward the ORR and better fuel cell performance have

* Corresponding author. Tel.: +82 41 860 1494; fax: +82 41 867 5396.
*E-mail address:* jsyu212@korea.ac.kr (J.-S. Yu).

0926-3373/$ – see front matter © 2008 Elsevier B.V. All rights reserved.
doi:10.1016/j.apcatb.2008.11.005

been demonstrated by the in-house made HCMS-supported Pt catalysts than the VC-supported ones under the identical DMFC cathode operation conditions.

## 2. Experimental

### 2.1. Preparation of HCMS carbons with various core size and shell thickness

HCMS carbons with various hollow core sizes and shell thickness have been prepared by replication through nanocasting of solid core/mesoporous shell (SCMS) silica [31]. Core sizes and shell thicknesses of HCMS carbons were controlled by the core sizes and shell thicknesses of the SCMS silica templates, respectively, while the micro- and mesoporosity of the HCMS carbons were controlled to some extent by the molar ratio of *n*-octadecyltrimethoxysilane ($C_{18}$-TMS) to tetraethyl orthosilicate (TEOS), and the amount of carbon precursor (i.e., phenol) incorporated into the SCMS silica templates. The silica sphere can be produced in various sizes by controlling the amount of TEOS added into the aqueous ammonia, and the SCMS silica can be produced in various sizes and various shell thicknesses by using the solid silica spheres with various sizes and adjusting the molar ratio of $C_{18}$-TMS to TEOS, respectively [32]. HCMS carbons with various hollow core sizes and shell thickness are denoted as $HCMS_{x/y}$, here *x* and *y* stand for hollow core size and mesoporous shell thickness in nm, respectively.

A typical synthesis route for SCMS silica with a core size of 310 nm and shell thickness of 53 nm is as follows. A total of 40 mL of aqueous ammonia (32 wt%) was added to a solution containing 1 L of ethanol and 80 mL of deionized water. After stirring at 30 °C for ca. 15 min, 60 mL of tetraethyl orthosilicate (TEOS) (98%, ACROS) was added to the above-prepared mixture, and the reaction mixture was stirred for ca. 6 h to yield uniform silica spheres. A mixture solution containing 50 mL of TEOS and 20 mL *n*-octadecyltrimethoxysilane ($C_{18}$-TMS) (90% tech., Aldrich) was added to the colloidal solution containing the silica spheres and further reacted for 1 h. The resulting octadecyl group-incorporated silica shell/solid core nanocomposite spheres were retrieved by centrifugation, dried at room temperature and further calcined at 823 K for 6 h under an oxygen atmosphere to produce the final uniform spherical SCMS silica particles. Aluminum was incorporated into the silicate framework through an impregnation method to produce acidic points on the surface of SCMS silica, which will catalyze polymerization of phenol and paraformaldehyde. A total of 1.0 g of SCMS silica was added to an aqueous solution containing 0.27 g of $AlCl_3{\cdot}6H_2O$ in 0.3 mL of water, and the resulting slurry was stirred for 30 min. The powder was dried in air at 353 K. Finally, the Al-impregnated SCMS silica was calcined at 823 K for 5 h in air to yield SCMS aluminosilicate.

A typical synthesis route for $HCMS_{300/50}$ carbon is as follows. 0.374 g of phenol was incorporated into the mesopores of 1.0 g of the SCMS template with core size of 310 nm and shell thickness of 53 nm by heating at 100 °C for 12 h under vacuum. The resulting phenol-incorporated SCMS template was reacted with paraformaldehyde (0.238 g) under vacuum at 130 °C for 24 h to yield a phenol-resin/SCMS aluminosilicate composite. The composite was heated at 1 K/min to 160 °C and held for 5 h under a nitrogen flow. The temperature was then ramped at 5 K/min to 950 °C and held for 7 h to carbonize the cross-linked phenol resin inside the mesopores of the SCMS structure. The dissolution of the SCMS template using 2.0N NaOH and washing in EtOH–$H_2O$ solution (volume ratio of EtOH to $H_2O$ = 1:1) produced the HCMS carbon. Slight shrinkage in core size and shell thickness of the HCMS carbon has been observed compared to those of the parent SCMS silica.

### 2.2. Surface characterization

$N_2$ adsorption and desorption isotherms were measured at 77 K on a KICT SPA-3000 Gas Adsorption Analyzer after the carbon was degassed at 423 K to 20 μTorr for 4 h. The specific surface areas were determined from nitrogen adsorption using the Brunauer–Emmett–Teller (BET) equation. The total pore volumes were determined from the amounts of gas adsorbed at the relative pressure of 0.99. Micropore (pore size $< 2$ nm) volumes of the porous carbons were calculated from the analysis of the adsorption isotherms using the Horvath–Kawazoe (HK) method. Pore size distribution (PSD) was derived from the analysis of the adsorption branch using the Barrett–Joyner–Halenda (BJH) method. Scanning electron microscopy (SEM) images were obtained using a Hitachi S-4700 microscope operated at an acceleration voltage of 10 kV. Transmission electron microscopy (TEM) was operated on EM 912 Omega at 120 kV, and high-resolution TEM (HR-TEM) images were obtained by using JEOL FE-2010 microscope operated at 200 kV. X-ray diffraction (XRD) analyses for carbon supported Pt catalysts were carried out with a Rigaku 1200 using Cu Kα radiation and a Ni β-filter and operating at 40 kV and 20 mA.

### 2.3. Preparation of carbon-supported catalyst electrodes

Carbon supported Pt (60 wt%) catalysts were synthesized at room temperature through impregnation method using $H_2PtCl_6{\cdot}6H_2O$ (Aldrich) as a metal precursor and $NaBH_4$ as a reducing agent. The catalyst inks were prepared by dispersing various carbon-supported Pt nanoparticles (or $Pt_{50}Ru_{50}$ (60 wt%)/VC (E-TEK) for the anode catalyst) into a mixture solution of an appropriate amount of deionized water and the required amount of 5 wt% Nafion ionomer (Aldrich). The Nafion ionomer contents in the catalyst layers were set as 25 wt%. Appropriate amounts of the catalyst inks were painted uniformly on Teflonized carbon paper (TGPH-090) and dried at 70 °C overnight. The catalyst loadings were 3 mg/cm$^2$ (based on $Pt_{50}Ru_{50}$ alloy only) at the anode and 5 mg/cm$^2$ at the cathode (based on Pt only). The membrane electrode assembly (MEA) was employed to construct a single fuel cell, which had been fabricated by hot-pressing a pretreated Nafion115 (Du-Pont) sandwiched by the anode and cathode.

### 2.4. Investigation of electrocatalytic activities of carbon-supported catalysts

For estimation of electrochemical active surface area of Pt in various carbon-supported Pt nanoparticles catalysts, cyclic voltammetry (CV) measurements were conducted with a three-electrode electrochemical cell at a scan rate of 25 mV/s in 0.5 M $H_2SO_4$ at room temperature. In all cases, Pt gauze was used as the counter electrode and Ag/AgCl as the reference one. Prior to any cyclic voltammetric measurements, the electrolyte solution was deaerated by high-purity nitrogen for 1 h and then stable voltammograms were recorded after 10 cycles. The working electrode was a thin layer of Nafion-impregnated catalyst cast on a glassy carbon disk (3 mm in diameter) embedded in a Teflon cylinder. The catalyst layer was prepared as follows. First, 5 mg of carbon-supported Pt catalyst (containing 60 wt% Pt) was dispersed in 1 mL of a solution of deionized water and ethanol (volume ratio of 1:1) and then mixed with 50 μL of Nafion solution (5 wt% Nafion). Next, the mixture was ultrasonicated for 1 h, and 10 μL of slurry was pipetted and spread on the top of the glassy carbon disk. Finally, the catalyst-coated glassy carbon electrode was dried at 70 °C for 2 h to yield a Pt loading of 0.126 mg/cm$^{2.}$

For evaluation of catalytic activity of various cathode catalysts toward ORR, CV and electrochemical impedance spectroscopy (EIS)

measurements were carried out at 30 °C using a two-electrode single cell with a 1.6 $cm^2$ cross-sectional catalyst area. After being humidified at a temperature of 15 °C higher than the cell operating temperature, $H_2$ and $O_2$ were supplied to the anode and cathode with zero back pressure at flow rates of 100 and 500 mL/min, respectively. Adsorbed $H_2$ gas on the supported Pt–Ru alloy catalyst worked as the counter and the pseudo-reference electrode (dynamic hydrogen electrode, DHE). The baseline for CV measurement was obtained by using HCMS carbon only as the working electrode. For the EIS analysis, an IM6ex impedance measurement unit (ZAHNER elektrik) was employed. The frequency range investigated was 100 kHz to 10 mHz, and the measurements were made with 10 mV of alternating current (ac) amplitude and 800 mV (vs DHE) of direct current (dc) bias.

Polarization performance tests were conducted using a single cell mode with 2.0 M of methanol fed to the anode at a feeding rate of 1 mL/min and $O_2$ or air fed to the cathode compartment with a flow rate of 300 mL/min.

## 3. Results and discussion

### 3.1. Structural characteristics of the HCMS carbons and the supported catalysts

Fig. 1 shows the representative TEM images of the HCMS carbons with various hollow core size and mesoporous shell thickness. Some HCMS carbon samples possess different core sizes (i.e., 300 and 350 nm) but the same shell thickness (i.e., 50 nm) while some of them have same core size (i.e., 300 nm) but different shell thickness (i.e., 40 and 50 nm). Furthermore, one sample (i.e., $HCMS_{170/30}$) has different core size and shell thickness with those of other samples. It is evident that the core size and/or shell thickness of the HCMS carbons can be controlled independently and easily through the control of the core size and/or shell thickness of the SCMS silica template, which can be realized by two separate synthesis processes, consisting of solid core formation by the Stöber method (first step) [33] and subsequent formation of the mesoporous shell by the Kaiser approach (second step) [34], namely, solid core size is controlled by the amount of added TEOS at the first step, and shell thickness is adjusted by the amount of TEOS and $C_{18}$-TMS at the second step.

Fig. 2 shows representative TEM images of the VC carbon-supported commercial E-TEK Pt nanoparticles (Fig. 2a), of the $HCMS_{300/50}$ (Fig. 2b), and of the HCMS carbon-supported Pt nanoparticles (Fig. 2c and d). The $HCMS_{300/50}$ carbon capsules existing as individual discrete particles were roughly uniform and spherical with particle diameter of ~400 nm as shown in Fig. 2b. The SEM image for a broken capsule shown in the inset indicates that the $HCMS_{300/50}$ capsule has a spherical hollow core. Both of the SEM and TEM images clearly show a hollow core of ~300 nm in diameter and mesoporous shell with thickness of ~50 nm.

The mesoporosity and surface properties of the $HCMS_{300/50}$ were examined by nitrogen isotherms as shown in Fig. 3, which can be classified as type IV typical of mesoporous materials. The HCMS carbon capsules revealed a narrow pore size distribution centred at 3.6 nm and exhibited a high BET surface area of 1870 $m^2/g$, and a total pore volume of 2.45 $cm^3/g$, which are mainly attributable to the presence of the mesopores in the shell (mesopore volume: 1.74 $cm^3/g$). Hence, each of the carbon capsules has a bimodal pore system composed of a spherical macroporous core and mesopores in the shell connecting the inside and outside of the hollow macroporous core. In contrast, the VC exhibits an appreciable amount of micropores (<2 nm) in addition to mesopores and macropores with varying sizes. As shown in the TEM image of Fig. 2c, although Pt aggregation was observed in certain areas, most of the Pt nanoparticles are dispersed homogenously as small, spherical and uniform particles over the $HCMS_{300/50}$ carbon support. The TEM image also indicates that the structural integrity of the HCMS capsules was pretty well reserved even after a high catalyst loading. The size of the Pt metal nanoparticles determined directly from the HR-TEM image shown in Fig. 2d at randomly selected regions for the HCMS carbon-supported catalyst was

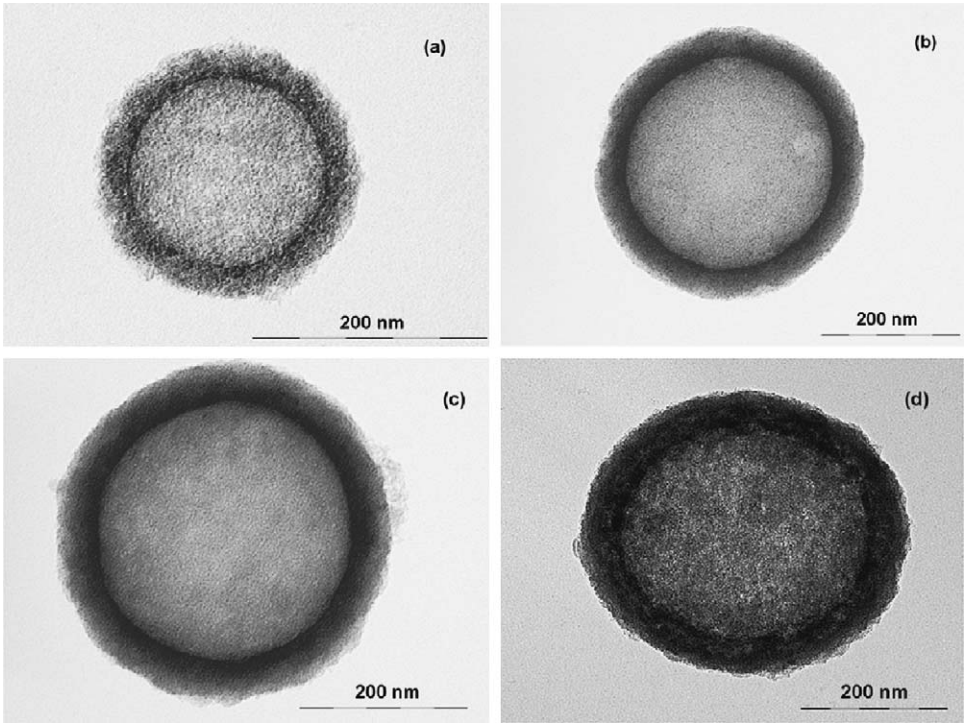


**Fig. 1.** Representative TEM images for the HCMS carbon samples with various core size and shell thickness: (a) $HCMS_{170/30}$, (b) $HCMS_{300/40}$, (c) $HCMS_{300/50}$ and (d) $HCMS_{350/50}$.

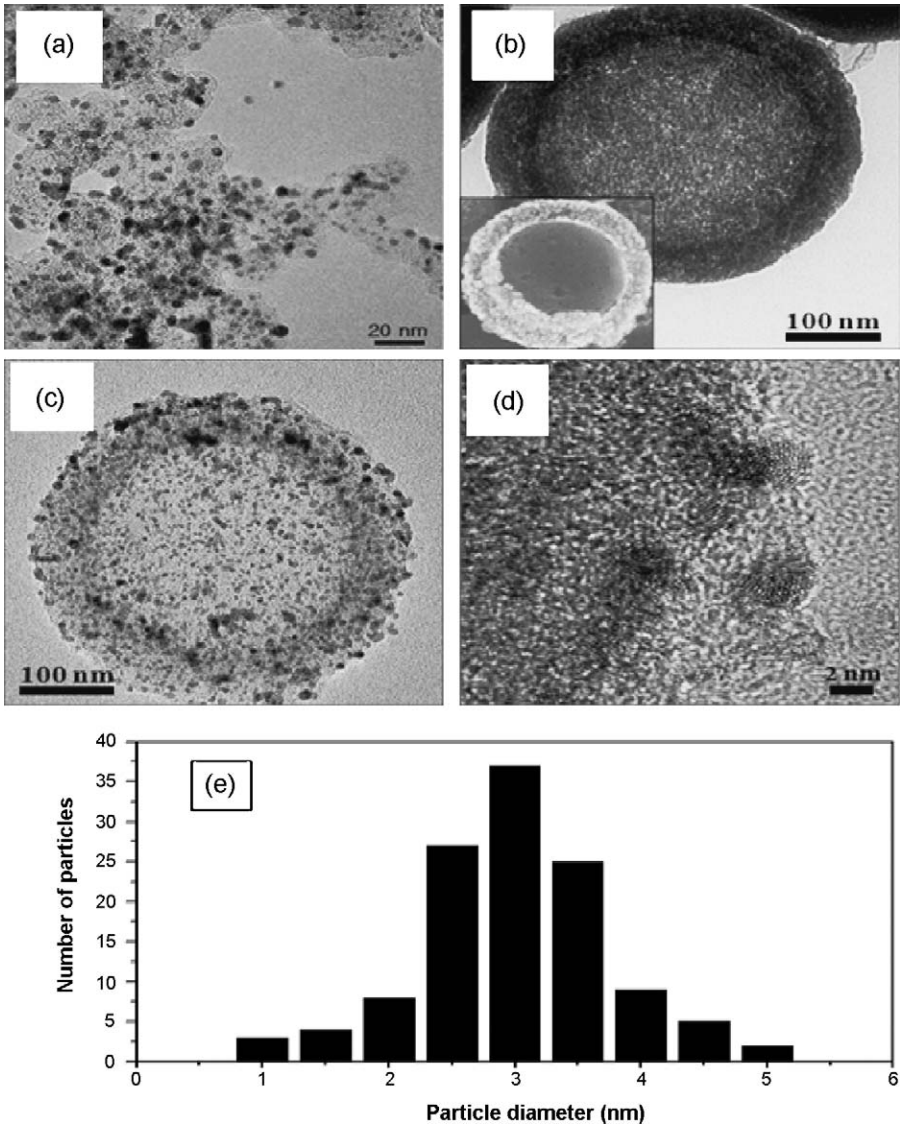


**Fig. 2.** TEM images of (a) commercial E-TEK Pt(60 wt%)/VC catalyst, (b) $HCMS_{300/50}$ carbon capsules, (c) Pt(60 wt%)/$HCMS_{300/50}$ catalyst, (d) HR-TEM image of Pt(60 wt%)/$HCMS_{300/50}$ catalyst, and (e) histogram of the particle size distribution for Pt nanoparticles as measured from 120 particles in TEM micrograph.

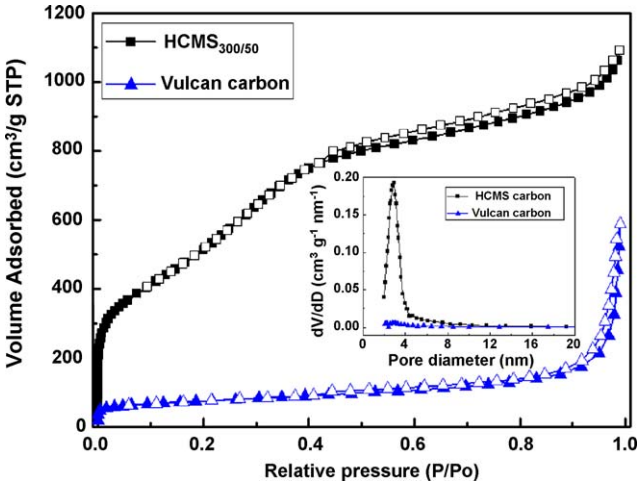


**Fig. 3.** Nitrogen adsorption–desorption isotherms obtained at 77 K and derived pore size distribution (PSD) for the $HCMS_{300/50}$ carbon. Solid circle: adsorption, empty circle: desorption.

approximately ~3 nm with narrow size distribution of from 2.5 to 3.5 nm as shown in Fig. 2e. The HR-TEM image shows small Pt crystalline particles dispersed in the HCMS carbon matrix. The data shown in Fig. 2c and d suggest that most Pt metal nanoparticles were dispersed uniformly on the HCMS carbon support with small particle size along with a narrow size distribution, which is expected to have good catalytic activity toward ORR under the cathode operation condition of DMFC.

Structural parameters for the HCMS carbons and VC derived from the $N_2$ adsorption–desorption isotherms are summarized in Table 1.

Typical XRD patterns of the $HCMS_{300/50}$ carbon- or the commercial carbon black VC-supported Pt (60 wt%) catalysts are shown in Fig. 4. All the supported Pt catalysts exhibit XRD patterns typical of the Pt fcc structure. The average particle size of 3.0 nm was calculated for the $HCMS_{300/50}$ carbon-supported Pt nanoparticles from the Pt (2 2 0) reflection of the XRD patterns according to the Scherrer equation, which is close to that (2.8 nm) of the commercial E-TEK Pt/VC and much smaller than that (3.7 nm) of the in-house Pt/VC, suggesting that it is possible to synthesize supported high-Pt loading catalyst with smaller nanoparticle size

**Table 1**
Surface structural parameters for the HCMS and VC carbons.

| Sample | $S_{BET}$ ($m^2$/g) | $V_{total}$ (cc/g) | $V_{meso}$ (cc/g) | $V_{micro}$ (cc/g) | Pore size (nm) |
|---|---|---|---|---|---|
| $HCMS_{170/30}$ | 1487 | 1.69 | 1.22 | 0.47 | 3.4 |
| $HCMS_{300/40}$ | 1535 | 1.93 | 1.38 | 0.55 | 3.5 |
| $HCMS_{300/50}$ | 1870 | 2.45 | 1.74 | 0.71 | 3.6 |
| $HCMS_{350/50}$ | 1736 | 2.12 | 1.51 | 0.61 | 3.5 |
| VC | 235 | 0.32 | 0.22 | 0.10 | – |

using a simple impregnation route if the support has large surface area, well-developed mesoporosity and narrow PSD.

### 3.2. Catalytic activities toward ORR of various catalysts

Electrochemical active surface areas were estimated from the integrated charge (after subtraction of capacitance contribution) in the hydrogen absorption region of the steady-state cyclic voltammogram in a supporting electrolyte and a monolayer hydrogen adsorption charge of 0.21 mC/$cm^2$ on Pt polycrystalline. As shown in Fig. 5, all Pt catalysts show the well-known hydrogen adsorption/desorption characteristics for carbon-supported platinum. A weak adsorption peak at ca. 0 V and a strong adsorption peak at ca. −0.15 V during the negative-going potential scan can be assigned to weakly and strongly bonded hydrogen adatoms, respectively [35]. Electrochemical surface areas were calculated as 65 $m^2$/g for Pt in the $HCMS_{300/50}$-supported Pt nanoparticles catalyst, which is much larger than that (45 $m^2$/g) for Pt in Pt(60 wt%)/VC (in-house), probably suggesting better utilization of Pt in the Pt(60 wt%)/$HCMS_{300/50}$ due to better distribution of Pt nanoparticle with smaller particle size on the $HCMS_{300/50}$ carbon than on the VC. This value is also larger than that (48 $m^2$/g) of Pt in commercial Pt(60 wt%)/VC (E-TEK). Certainly, the larger Pt electrochemical active surface area is favourable for the higher ORR activity since the surface area can be used to evaluate the intrinsic electrocatalytic activity of a Pt-based catalyst.

The ORR activities of various Pt cathode catalysts were first evaluated by CV measurement using a single cell mode with pure $O_2$ fed to the cathode. Commercial unsupported Pt black from Johnson-Matthey, which is frequently used as a cathode catalyst in DMFCs, was investigated for the sake of comparison. In addition, one of the state-of-the-art catalysts, E-TEK Pt (60 wt%)/VC was also examined for its ORR activity. Fig. 6 shows the cyclic voltammograms obtained for various Pt catalysts under oxygen atmosphere.

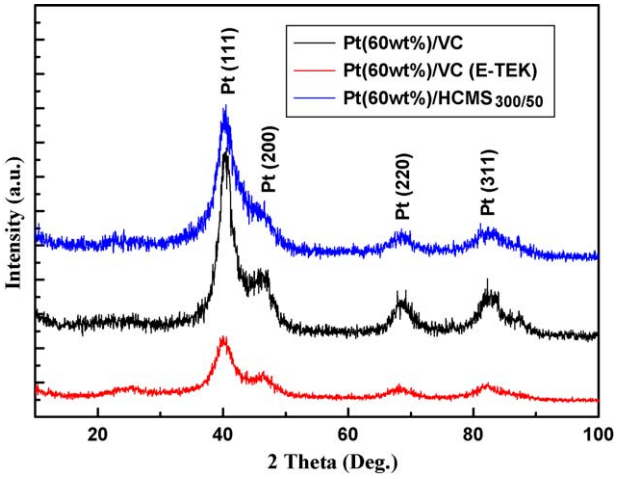


**Fig. 4.** Typical XRD patterns for the $HCMS_{300/50}$ carbon- or the commercial carbon black VC-supported Pt (60 wt%) catalysts.

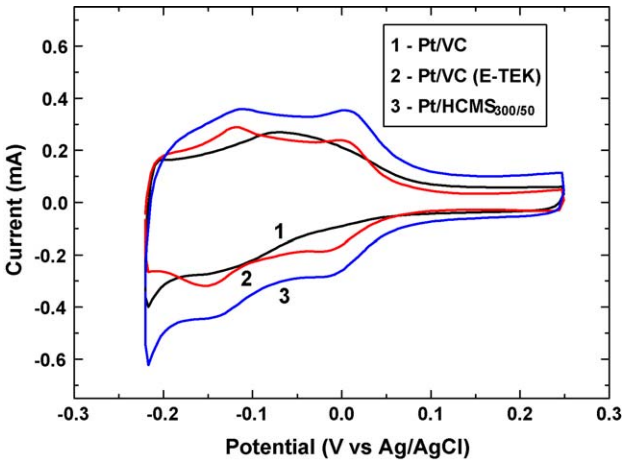


**Fig. 5.** Hydrogen electrosorption voltammetric profiles obtained from various supported Pt (60 wt%) catalysts in 0.5 M $H_2SO_4$ at room temperature with a scan rate 25 mV/s. Pt gauze was used as the counter electrode and Ag/AgCl as the reference one.

The onset potentials which correspond to a starting point of ORR for each catalyst were 870, 895, and 928 mV (vs DHE) for the unsupported Pt black (J.M.), Pt(60 wt%)/VC (E-TEK), and Pt(60 wt%)/$HCMS_{300/50}$, respectively. This indicates that supported Pt catalysts start the ORR earlier than the unsupported Pt black, which is attributable to the supporting effect of the catalyst supports, which favours the formation of highly dispersed Pt nanoparticles with small particle size. In addition, the $HCMS_{300/50}$-supported Pt starts ORR earlier than the VC-supported one (in-house), probably suggesting the contribution of the Pt nanoparticle size on the onset potential. At 0.8 V (vs DHE), Pt/$HCMS_{300/50}$ exhibited a current response of 232 mA/$cm^2$, which is much greater than that (140 mA/$cm^2$) for the Pt/VC (E-TEK) catalyst, implying that Pt/$HCMS_{300/50}$ catalyst has higher electrocatalytic activity toward the ORR than commercial E-TEK one.

The ORR activities of various Pt cathode catalysts were further confirmed by Nyquist plots shown in Fig. 7. Two high frequency (HF) capacitive loops and one low frequency (LF) inductive loop (i.e., 407–10 mHz) were observed. The first small HF loop (>419 Hz) corresponds to the ohmic process within the porous structure of the electrode and membrane [36] while the second HF loop (i.e., 419 Hz to 407 mHZ) and the inductive loop (i.e., 407–

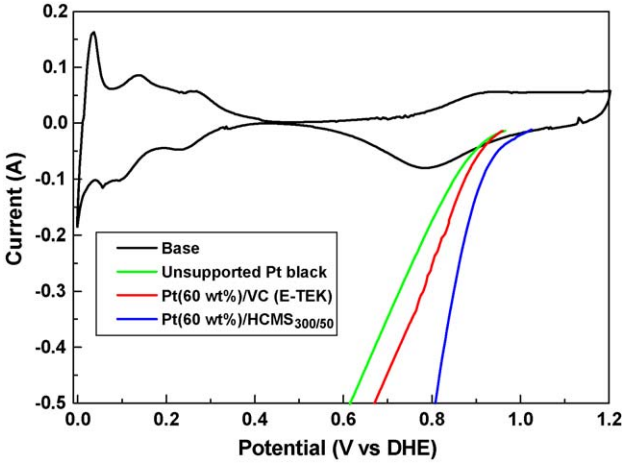


**Fig. 6.** Cyclic voltammograms obtained for various Pt catalysts under oxygen atmosphere with a scan rate of 10 mV/s. Potentials were measured with reference to dynamic hydrogen electrode (DHE).

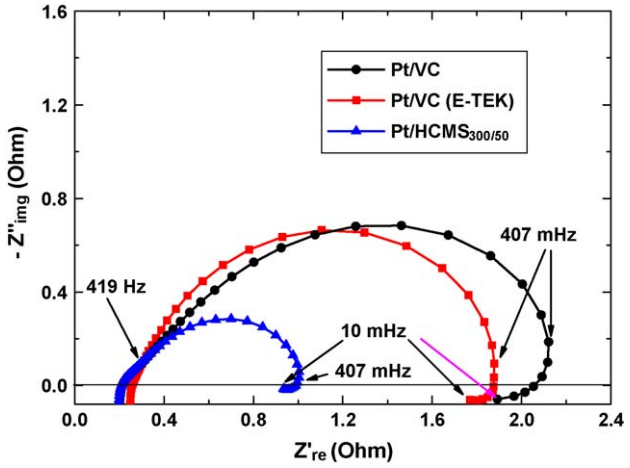


**Fig. 7.** Typical Nyquist plots for the $HCMS_{300/50}$ or VC-supported Pt (60 wt %) catalysts, dc bias: 0.8 V (vs DHE), ac amplitude: 10 mV.

10 mHz) correspond to ORR kinetics [36], and relaxation and diffusion of adsorbed oxygenated intermediate species [37]. It is clear that when the catalyst support changes from the VC to $HCMS_{300/50}$ carbon, the diameter of the second HF loop (i.e., 419 Hz to 407 mHz) decreases dramatically, indicating that the ORR charge-transfer resistance is much smaller at the HCMS carbon-supported Pt cathode catalyst. This finding is in good agreement with the result derived from the CV measurements for the ORR activities of the various Pt catalysts in Fig. 6.

### 3.3. Polarization performance of DMFCs using various supported Pt cathode catalysts

The ORR activities of various supported Pt cathode catalysts were finally evaluated by polarization performance examination using a single cell mode with methanol fed to the anode and $O_2$ or air fed to the cathode. Fig. 8 shows the polarization performance for DMFCs using various carbon-supported Pt (60 wt%) cathode catalysts at 30 °C (Fig. 8a) and 60 °C (Fig. 8b) with $O_2$-fed mode and at 30 °C with air-fed mode (Fig. 8c). Compared with the performance at relatively high temperature (i.e., 60 °C), the performance of fuel cell at relatively low temperature (i.e., 30 °C) is more concerned due to their most potential applications of the DMFCs in portable or small electronic devices requiring low temperature operation. In the low current density region, the fuel cell polarization is primarily attributable to sluggish charge transfer involved in the ORR at the cathode surface. Thus, it is evident that at 0.4 V the activation polarization is mainly affected by activity of the catalyst. At 30 °C and at 0.4 V with $O_2$-fed mode, the $Pt/HCMS_{300/50}$ catalyst shows a current density of 119 mA/cm$^2$, which is ca. 32% higher than that (i.e., 90 mA/cm$^2$) of the Pt/VC (E-TEK) catalyst. Appreciably smaller activation polarization was observed from the HCMS-supported Pt catalyst than the VC-supported ones, suggesting more rapid ORR kinetics on the surface of the former in agreement with conclusions drawn from the CV measurements in Fig. 6 and Nyquist plots in Fig. 7 for the ORR activities of the various Pt catalysts. In addition, the $Pt/HCMS_{300/50}$ catalyst exhibits a much higher maximum power density (i.e., 90 mW/cm$^2$) than that (i.e., 47 mW/cm$^2$) of the in-house Pt/VC and that (i.e., 50 mW/cm$^2$) of the Pt/VC (E-TEK) catalyst. This corresponds to an enhancement of ca. 91% compared with the Pt/VC (in-house) and of 80% compared with that of the state-of-the-art E-TEK Pt/VC catalyst. Similar improvement in fuel cell performance was also observed in power delivery at 60 °C as shown in Fig. 8b. The $Pt/HCMS_{300/50}$ catalyst exhibits a maximum

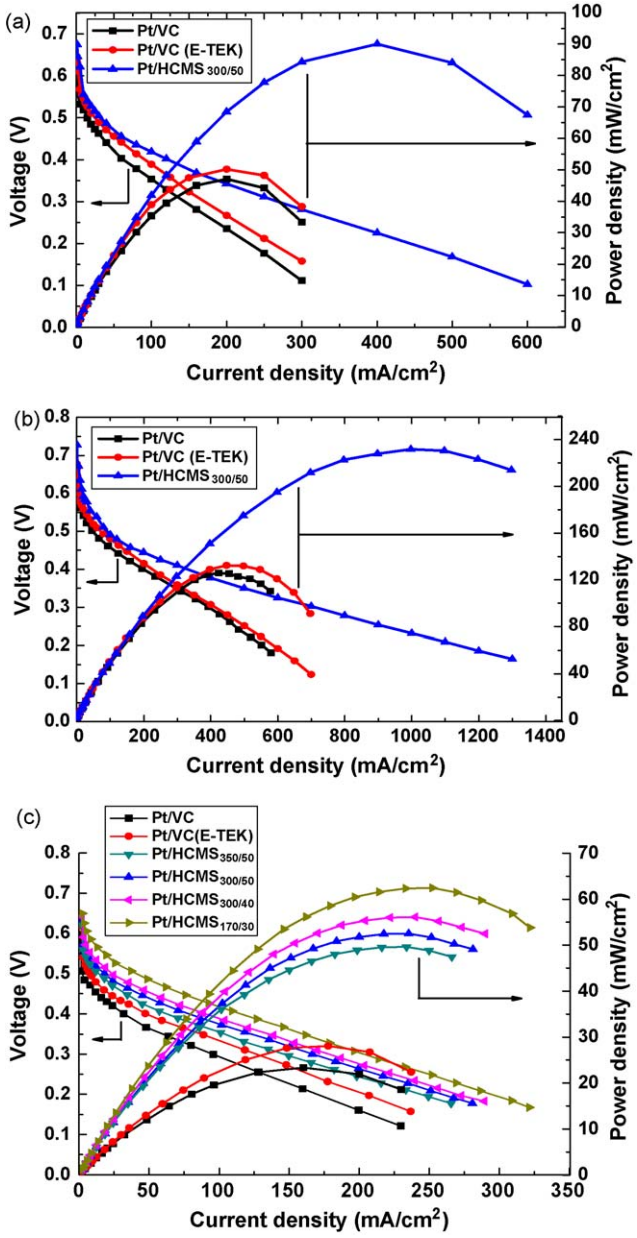


**Fig. 8.** Polarization and power density plots for DMFC using various carbon-supported Pt(60 wt%) cathode catalysts at 30 °C (a) and 60 °C (b) with $O_2$-fed cathode mode and at 30 °C with air-fed cathode mode (c).

power density of 232 mW/cm$^2$, which is much higher than that (i.e., 126 mW/cm$^2$) of the in-house Pt/VC and that (i.e., 132 mW/cm$^2$) of the Pt/VC (E-TEK). At 30 °C with air-fed cathode mode, the maximum power density for the $Pt/HCMS_{300/50}$ is 53 mW/cm$^2$, corresponding to an enhancement of ca. 128% compared with that (i.e., 22 mW/cm$^2$) of the Pt/VC (in-house) and of ca. 89% compared with that (i.e., 28 mW/cm$^2$) of the Pt/VC (E-TEK). In addition, other HCMS carbon-supported Pt catalysts also demonstrated considerable enhancement in power delivery compared with the VC-supported ones. Evidently, whether the HCMS carbons have varied core size and (or) shell thickness, the HCMS-supported Pt cathode catalysts obviously outperformance the VC-supported ones, implying that the reproducibility and reliability of the Pt/HCMS catalysts have been guaranteed.

It is noteworthy that compared with the data at the identical temperature (i.e., 30 °C) with $O_2$-fed mode, much lower specific

power densities were observed for the $HCMS_{300/50}$ carbon- or VC-supported Pt catalysts with air-fed mode. The lower specific power density with air-fed mode mainly results from the mass-transport loss incurred by poor $O_2$-transport through the diffusion medium and the electrode layer. Interestingly, lower mass-transport loss was observed for the $HCMS_{300/50}$ carbon-supported Pt catalyst compared with the VC-supported catalysts. For the $HCMS_{300/50}$ carbon-supported Pt catalyst, specific power density decreases to 53 $mW/cm^2$ (with air-fed mode) from 90 $mW/cm^2$ (with $O_2$-fed mode), corresponding to a reduction of ca. 41%, while for the in-house VC-supported Pt catalyst, specific power density decreases to 22 $mW/cm^2$ (with air-fed mode) from 47 $mW/cm^2$ (with $O_2$-fed mode), corresponding to a reduction of ca. 53%.

The considerable improvement in the electrocatalytic activity and fuel cell performance is attributable to the supporting effect of the HCMS carbon, related to its unique structural properties. Larger specific surface area and mesopore volume of the HCMS carbon favour a better dispersion of the supported Pt nanoparticles with smaller particle size, resulting in higher electrochemically accessible surface area of Pt in the supported catalyst and accordingly, higher electrocatalytic activity toward ORR. This is main reason for the improvement of the electrocatalytic activity and fuel cell performance. In addition, the well-developed bimodal nanoporous structure with the mesopores in the shell open to the outer surface and to the inner hollow macroporous core provides an open highway network around the Pt catalyst for efficient mass transport particularly in the case of air fed to the cathode. Furthermore, the 3D large interstitial spaces between the packed spherical carbon particles, unique in this system, are open to the mesoporous channels, serving as primary fast pathways for the delivery of the reactants and products. From the SEM images of cross-section of the interface of electrolyte and catalyst layer shown in Fig. 9, it is found that the VC-supported Pt catalyst layer is tightly packed with not much space in the layer while the HCMS-supported one exhibits large channel (space) in the catalyst layer due to the larger particle size of the HCMS carbon with spherical morphology. For the former catalyst, Pt nanoparticles are closely covered by the VC support, which may hinder the mass transfer in the Pt/VC catalyst layer. In contrast, there still exits large pores or channels in the Pt/HCMS catalyst layer, and the Pt nanoparticles are not readily covered by the HCMS support and more likely exposed to the electrolyte, favouring the access of the reactant into the catalyst layer and the product removal. Similar effect from the interstitial spaces between the packed spherical carbon particles has been recently reported by Liu et al. [38], namely, mesocarbon microbeads (MCMB)-supported Pt-Ru catalyst has demonstrated enhanced catalytic activity toward methanol oxidation compared with the VC-supported one although MCMB has a much larger particle size (ca. 1–40 μm) than the VC (ca. 40 nm). They attributed the high catalytic activity of Pt-Ru/MCMB to the change of the structure of catalyst layer when compared with the VC supported catalysts. Through the morphologies of cross-section of the interface of electrolyte and catalyst layer, they found that the VC-supported catalyst has a tight contact with the Nafion membrane, which may cause the difficulty in mass transfer in the catalyst layer of electrochemical reaction. Interestingly, the MCMB-supported catalyst shows large pores or channels in the catalyst layer, and the Pt-Ru alloy particles have easy access to the electrolyte, improving the utilization of the catalyst. It is likely that proper amount of spaces and channels in the catalyst layer are necessary to favour the mass transfer.

Although the HCMS carbon-supported Pt catalysts outperformance the VC-supported ones, there is still a room for further improvement in performance of DMFC using HCMS carbon-supported Pt catalyst. Compared with VC, HCMS carbons have larger particle size (230–450 nm), which may cause a thicker catalyst layer in the electrode. From Fig. 8c, it is clear that the hollow core size and mesoporous shell thickness of the HCMS carbon samples have impacts on the polarization performance of the supported Pt catalysts, namely, with decreasing HCMS particle size (i.e., decreasing hollow core size or shell thickness), power delivery of the HCMS-supported Pt catalyst increases, which may be mainly contributable to the decreased thickness of Pt catalyst layer because no appreciable difference between the dispersion degrees and particle sizes of the supported Pt nanoparticles was observed for the HCMS-supported catalysts from their TEM images (not shown), resulting in a decreased mass transport resistance. Hence, in order to further improve fuel cell performance it is necessary and important to develop HCMS carbon with smaller hollow core size and thinner mesoporous shell and employ them to support Pt with higher metal loading such as 80 wt% to shorten diffusion path. This work is under process.

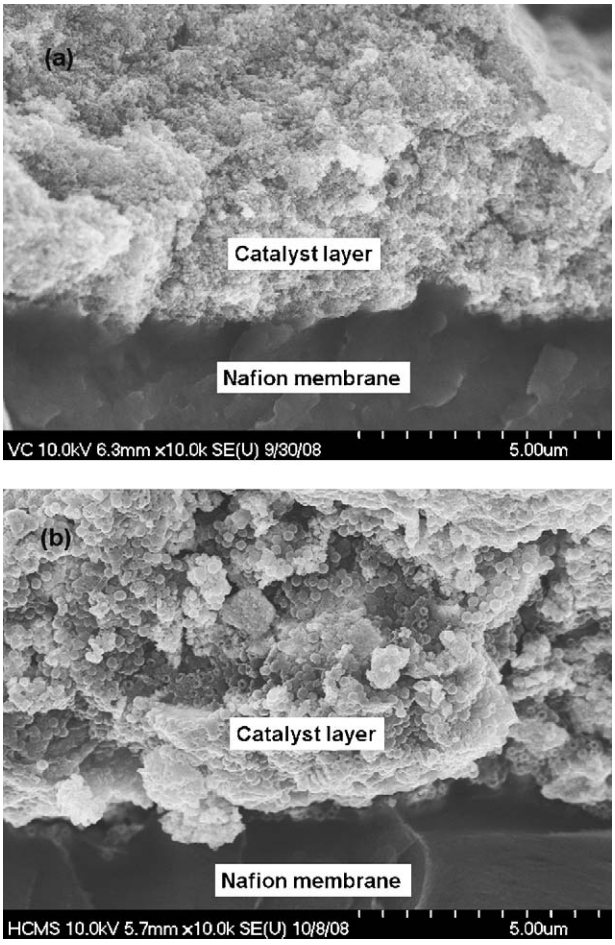


**Fig. 9.** SEM images of cross-section of the interface of electrolyte and catalyst layer. (a) VC-supported Pt (60 wt %) catalyst, (b) HCMS-supported Pt (60 wt %) catalyst.

## 4. Conclusions

In this work, HCMS carbon-supported Pt catalyst exhibits higher electrocatalytic activity toward ORR than the VC-supported Pt cathode catalysts, which is contributable to larger surface area and mesoporous volume of the HCMS carbon. In addition, compared with the VC-supported Pt cathode catalysts much higher power can be delivered by the HCMS carbon-supported Pt catalyst especially in the case of air fed to the cathode, which is closely related to the unique structural properties of the HCMS

carbon capsules mainly including large surface area, well-developed bimodal porosity and interstitial void channels. Based on the results obtained, the HCMS carbon is an excellent cathode catalyst support in DMFC.

The core sizes, shell thickness and porosity and surface morphology of the HCMS carbon capsules can be controlled by monitoring the size of the silica sphere core, the amount and ratio of TEOS and $C_{18}$-TMS added, thermal treatment and carbon precursors and their blend [32,39]. The work in the direction of the structure control of the HCMS carbon capsules and systematic investigation into the effects of HCMS carbon with varying porosity and (or) pore diameter on catalytic activity of the supported catalyst and DMFC performance are under progress.

## Acknowledgements

The authors thank KICOS for financial support toward Korean–Italian Joint Research Project and the Korean Basic Science Institute at Jeonju, Chuncheon and Deajeon for SEM and TEM measurements. The authors also thank Mr. Minwoo Kim for BET and XRD measurements.

## References

[1] J. Han, E.S. Park, J. Power Sources 112 (2002) 477.
[2] H. Chang, J.R. Kim, J.H. Cho, H.K. Kim, K.H. Choi, Solid State Ionics 148 (2002) 601.
[3] A. Blum, T. Duvdevani, M. Philosoph, N. Rudoy, E. Peled, J. Power Sources 117 (2003) 22.
[4] C.Y. Chen, P. Yang, J. Power Sources 123 (2003) 37.
[5] D. Kim, E.-A. Cho, S.-A. Hong, I.-H. Oh, H.-Y. Ha, J. Power Sources 130 (2004) 172.
[6] H. Qiao, M. Kunimatsu, T. Okada, J. Power Sources 139 (2005) 30.
[7] M.V. Martínez-Huerta, S. Rojas, J.L. Gómez de la Fuente, P. Terreros, M.A. Peña, J.L.G. Fierro, Appl. Catal. B: Environ. 69 (2006) 75.
[8] M.A. Scibioh, I.-H. Oh, T.-H. Lim, S.-A. Hong, H.-Y. Ha, Appl. Catal. B: Environ. 77 (2008) 373.
[9] Z.-C. Tang, G.-X. Lu, Appl. Catal. B: Environ. 79 (2008) 1.
[10] C. Lim, C.Y. Wang, J. Power Sources 113 (2003) 145.
[11] L. Liu, C. Pu, E.S. Smotkin, Electrochim. Acta 43 (1998) 3657.
[12] P.J. Britto, K.S.V. Santhanam, A. Rubio, J.A.A. Alonso, P.M. Ajayan, Adv. Mater. 11 (1999) 154.
[13] A.S. Arico, S. Srinivasan, V. Antonucci, Fuel Cells 2 (2001) 1.
[14] M.K. Ravikumar, A.K. Shukla, J. Electrochem. Soc. 143 (1996) 2601.
[15] W. Li, C. Liang, W. Zhou, J. Qiu, Z. Zhou, G. Sun, Q. Xin, J. Phys. Chem. B 107 (2003) 6292.
[16] Z.Q. Tian, S.P. Jiang, Y.M. Liang, P.K. Shen, J. Phys. Chem. B 110 (2006) 5343.
[17] W. Li, X. Wang, Z. Chen, W. Waje, Y. Yan, Langmuir 21 (2005) 9386.
[18] Z. Liu, J. Lee, W. Chen, M. Han, L. Gan, Langmuir 20 (2004) 181.
[19] T. Matsumoto, T. Komatsu, K. Arai, T. Yamazaki, M. Kijima, H. Shimizu, Y. Takasawa, J. Nakamura, Chem. Commun. (2004) 840.
[20] T. Maiyalagan, Appl. Catal. B: Environ. 80 (2008) 286.
[21] C. Bessel, K. Laubernds, N. Rodriguez, R. Baker, J. Phys. Chem. B 105 (2001) 1115.
[22] E.S. Steigerwalt, G.A. Deluga, C.M. Lukehart, J. Phys. Chem. B 106 (2002) 760.
[23] G.S. Chai, S.B. Yoon, J.-S. Yu, Carbon 43 (2005) 3028.
[24] T. Yoshitake, Y. Shimakawa, S. Kuroshima, H. Kimura, T. Ichihashi, Y. Kubo, Physica B 323 (2002) 124–126.
[25] M. Kim, S. Hwang, J.-S. Yu, J. Mater. Chem. 17 (2007) 1656.
[26] K.-Y. Chan, J. Ding, J. Ren, S. Cheng, K.Y. Tsang, J. Mater. Chem. 14 (2004) 505.
[27] J.-S. Yu, S. Kang, S.B. Yoon, G. Chai, J. Am. Chem. Soc. 124 (2002) 9382.
[28] F. Su, X.S. Zhao, Y. Wang, J. Zeng, Z. Zhou, J.Y. Lee, J. Phys. Chem. B 109 (2005) 20200.
[29] Y. Liu, X. Qiu, Y. Huang, W. Zhu, G. Wu, J. Appl. Electrochem. 32 (2002) 1279.
[30] G.S. Chai, S.B. Yoon, J.H. Kim, J.-S. Yu, Chem. Commun. (2004) 2766.
[31] S.B. Yoon, K. Sohn, J.Y. Kim, C.-H. Shin, J.-S. Yu, T. Hyeon, Adv. Mater. 14 (2002) 19.
[32] M.-S. Kim, S.-B. Yoon, K. Sohn, J.-Y. Kim, C.-H. Shin, T. Hyeon, J.-S. Yu, Micropor. Mesopor. Mater. 63 (2003) 1.
[33] W. Stöber, A. Fink, E. Bohn, J. Colloid Interface Sci. 26 (1968) 62.
[34] C. Kaiser, K.K. Unger, German Patent DE-195 30031 A1 (1997).
[35] D.C. Papageorgopoulos, M. Keijzer, J.B.J. Veldhuis, F.A. de Bruijn, J. Electrochem. Soc. 149 (2002) A1400.
[36] H. Huang, W.-K. Zhang, M.-C. Li, Y.-P. Gan, J.-H. Chen, Y.-F. Kuang, J. Colloid Interface Sci. 284 (2005) 593.
[37] O. Antoine, Y. Bultel, R. Durand, J. Electroanal. Chem. 499 (2001) 85.
[38] Y. Liu, X. Qiu, Y. Huang, W. Zhu, J. Power Sources 111 (2002) 160.
[39] G. Buchel, K.K. Unger, A. Matsumoto, K. Tsutsumi, Adv. Mater. 10 (1998) 1036.